



Regular Articles

All-fiber fast acousto-optic temporal control of tunable optical pulses

Ricardo E. da Silva^{a,c,*}, Egor Manuylovich^a, Namita Sahoo^a, Marcos A.R. Franco^c, Hartmut Bartelt^b, David J. Webb^a^a Aston Institute of Photonic Technologies (AIPT), Aston University, Birmingham B4 7ET, UK^b Leibniz Institute of Photonic Technology (IPHT), Jena 07745, Germany^c Institute for Advanced Studies (IEAv), São José dos Campos 12228-001, Brazil

ARTICLE INFO

Keywords:

Acousto-optic modulators
Fiber Bragg gratings
Suspended core fibers
Tunable optical pulses
Numerical simulation

ABSTRACT

We demonstrate a new all-fiber electrically tunable modulation method which significantly reduces the response time of a Bragg grating acousto-optic modulator. A 4 cm long device is fabricated with a 1 cm grating inscribed in a suspended core fiber. An acoustic pulse train is switched out of phase along the fiber, damping unwanted natural resonant vibrations inside the grating. The device rise time is decreased from 56 to 9 μ s by tuning the duty cycle of the driven electrical signal, contributing to achieve the shortest switching time of 15.6 μ s. This tunable temporal response reveals unique features to change the profile of optical pulses. High pulse modulation depths are achieved employing a compact acousto-optic modulator, pointing to fast switching of all-fiber photonic devices.

1. Introduction

Temporal control of optical pulses has remarkable applications in all-optical signal processing [1], slow and fast light [2–5], pulse shaping [6,7], microwave photonics [8], high-resolution strain and temperature fiber sensors [9] and narrow linewidth fiber lasers [10]. The interaction of two counter-propagating optical waves and longitudinal acoustic waves (phonons) in long fiber lengths enables the dynamic tuning of the pulses' rise time by means of stimulated Brillouin scattering [3]. Alternatively, devices employing short fiber lengths are important for practical applications since the pulses' time delay is basically defined by the transit time of the optical signal within the fiber [4,5]. In this case, fiber Bragg gratings (FBGs) are attractive to induce significant temporal delays of the light over short distances (0.6–20 cm) [4,9,11]. Superstructure and π phase shifted FBGs efficiently shape optical pulses in short fiber lengths employing low power sources [5,7–9]. These gratings are inscribed along the fiber with one or multiple π phase shifts, or with the modulated refractive index being apodized with a Gaussian or sinc profile [6–8,12]. Permanent modulation of grating properties results in exceptional temporal integrators [6], differentiators [7] and fractional Hilbert transformer (FHT) filters [8] for reconfigurable signal processors [1]. In general, the filter order increases by decreasing the modulation amplitude of the grating refractive index [7]. Nevertheless, the filter order is usually limited due to the grating fabrication complexity [7].

High power optical pulses (gap solitons) have been employed to induce an effectively long optical path length inside the grating [4]. The optical pulses are delayed by changing the pump power and detuning the pulse in relation to the grating reflection edge.

Overall, most of the proposed devices are usually limited in their ability to rapidly tune the optical properties. In general, high-power pump sources and high voltage-based techniques cause significant temperature-induced changes in the fiber refractive index. Consequently, the device response time is usually limited to the milliseconds range because of the slow material heating and cooling process [13]. Besides, the combination of long fiber lengths, bulk-type modulators and free-space optics may induce undesirable insertion losses, increasing the setup complexity, the number of components, and the costs [2,3,9]. In contrast, all-fiber acousto-optic modulators (AOMs) can change signal optical properties, such as power, wavelength and polarization, with low insertion loss, employing a small number of components [10,14–24]. In particular, the interaction of acoustic waves and FBGs has successfully been employed in dynamic optical filters, fiber sensors and Q-switched and mode-locked fiber lasers [10,15,20,22–24], enabling response times from 40 to 500 μ s [15,17–21].

An ideal acousto-optic device switching ON/OFF an acoustic signal would instantaneously modulate a rectangular optical pulse as illustrated in Fig. 1(a). However, the temporal response of practical acousto-optic devices depends on the damping time of free natural resonant

* Corresponding author at: Aston Institute of Photonic Technologies (AIPT), Aston University, Birmingham B4 7ET, UK.

E-mail address: r.da-silva@aston.ac.uk (R.E. da Silva).

vibrations remaining in the fiber after the switching ON/OFF of the applied acoustic stress (step amplitude variation) [25]. The natural resonances modulate the pulse amplitude inducing periodic temporal peaks (Fig. 1(b)). The temporal period of the fundamental sinusoidal wave resonance is determined by the fiber length L and material as, $\tau_R = 4L(\rho/Y)^{1/2}$, in which, ρ is the density and Y is the Young's modulus [25]. This resonance is damped after a transition time, usually given by the rising or falling time of the mechanical stress until reaching a steady state. Reduction of this transition time shortens the pulse duration, increasing for example the maximum repetition rate and output power of acoustically modulated pulsed fiber lasers [15,20]. In this paper, we experimentally and numerically demonstrate a new AOM technique which induces a phase-shift in the natural resonances (Fig. 1(c)), allowing tuning, and significantly reducing, the rise and switching time of an acousto-optic device. Additionally, the amplitude modulation of optical pulses in FBGs caused by the fiber's natural resonant vibrations is investigated in detail.

2. Materials and methods

Fig. 2(a) illustrates the fabricated modulator, basically composed of a piezoelectric transducer (PZT), an acoustic silica horn and a segment of a highly birefringent suspended core fiber (HB-SCF). The HB-SCF in Fig. 2(b) is 124 μm in diameter, containing two similar pure silica birefringent cores ($7.7 \mu\text{m} \times 4 \mu\text{m}$) surrounded by four air holes of 40–43 μm diameter, separated by silica bridges of 2.7 μm thickness. A 1 cm long FBG is inscribed in the HB-SCF by means of a femtosecond laser using a phase mask interferometer as described in [26]. The HB-SCF's large air holes significantly strengthen the interaction of acoustic waves and the grating in the fiber core [22,24]. The interaction of the HB-SCF's "fast X" and "slow Y" polarization modes with the grating results in two reflected bands centered at $\lambda_X = 1540.7 \text{ nm}$ and $\lambda_Y = 1540.9 \text{ nm}$ (unmodulated spectrum in Fig. 2(c)). The PZT disc is 3 mm in diameter and 2 mm in thickness. The hollow silica horn is tapered in diameter from 1.06 mm to 200 μm along 1.4 cm length (tip of 150 μm inner diameter). The horn is connected to the PZT and to the HB-SCF by means of a glass adhesive. The modulator ends are fixed, resulting in a total device length of 4 cm.

A rectangular pulse train with a voltage amplitude of 10 V and frequency of $f = 469 \text{ kHz}$ is applied to the PZT with a signal generator (SG). The PZT generates standing longitudinal acoustic waves which are coupled to the fiber by the horn. The acoustically induced strain modulates the grating reflectivity switching ON and OFF the polarization peaks λ_X and λ_Y at twice the applied acoustic frequency ($f = 938 \text{ kHz}$) [22]. Fig. 2(c) shows the unmodulated and modulated FBG spectra normalized to the maximum reflectivity, as recorded by the optical spectrum analyzer (OSA).

Although it is not visible, the maximum temporal modulation depth of our device might be higher than $\Delta\eta = 90\%$ even though the variation of the reflectivity indicated by the OSA only reached 61% at 10 V; this is because our OSA could not measure the instantaneous modulation depth

of the fast modulated optical signal at $f = 938 \text{ kHz}$, but only showed its average value in Fig. 2(c) – details about temporal and average reflectivity are shown in [27]. Overall, this spectral modulation indicates a significantly high acousto-optic efficiency for a compact device (4 cm) and low applied voltage (10 V). One core of the HB-SCF is spliced to the core of a standard single mode fiber (SMF) of a circulator. The temporal response of the grating spectrum is characterized by tuning a CW laser (TL) at λ_X , as illustrated in Fig. 2(c) (green dashed line). The power reflected by the grating is measured with a photodetector (PD) and an oscilloscope (OSC). Acoustic pulse trains are generated by inducing a temporal gap of constant positive polarization of +10 V (duty cycle OFF) in the rectangular electrical signal (a detail of the electrical signal is further shown in Fig. 6). Fig. 2(d) shows the temporal response of the applied electrical pulses (blue signal) and the FBG modulated reflected power at the duty cycle ON (Dc) of 89.2%.

The maximum modulation depth $\Delta\eta_t = 1$ is normalized to the maximum voltage of the photodetector, corresponding the peak reflected power of the unmodulated grating. The minimum level $\Delta\eta_t = 0$ corresponds to the combined average of the photodetector's background noise and the high frequency modulated signal at $f = 938 \text{ kHz}$. This averaging allowed better evaluation of the temporal properties of the low frequency amplitude modulated optical pulses and fundamental mechanical resonance during the duty cycle OFF. The pulse width Pw_t (full width at half maximum – FWHM) of the reflected optical pulse is tuned by changing the duty cycle from $Dc = 70.1$ to 99.4% (6.4% steps, 3.8% last step) at a fixed repetition rate of $Rr = 30 \text{ Hz}$ (period of $T = 33 \text{ ms}$). The pulses are also simulated along the fiber and FBG by means of the finite element method and transfer matrix method, considering the methodology and material parameters described in [16,25]. Fig. 2(b) shows the simulated power distribution of the fundamental fast X mode in the SCF's cores. The red arrows in the simulation indicate the X polarization of the electric field in the fiber cores (the simulated fiber cores and mode profiles are rotated about 45° to fit in Fig. 2(b)).

3. Results and discussion

Fig. 3(a) shows the temporal modulation of the fast mode X at λ_X for the considered Dc range. Although it is not shown, similar results are also observed for the slow mode Y at λ_Y . Note in Fig. 3(b) that the pulse width is linearly tuned from $\Delta Pw_t = 9.9$ to 0.2 ms. The fast mode reflectivity is recovered to 100% at $Dc = 70.1\%$, gradually decreasing with increasing Dc . For low Dc values, the time interval between two pulse trains is rather large, allowing the grating reflectivity a full or almost complete recovery. The grating recovery (characterized by the modulation depth) is triggered by turning the acoustic pulses OFF during the temporal gap between two acoustic pulses being ON. From $Dc = 70.1\%$ upwards, the remaining oscillations in the fiber modulating the grating prevent its reflectivity to recovery before the next acoustic pulse. Consequently, the increasing Dc reduces the temporal gaps, the grating recovery, and the optical pulse modulation depth. The optical pulse amplitude variation is perceived in Fig. 3(a) showing smooth response

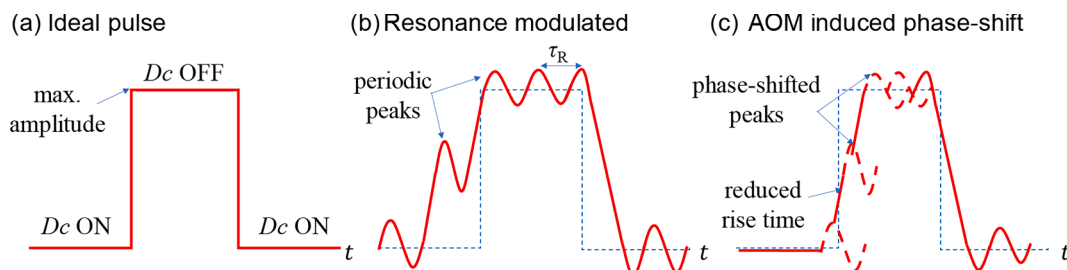


Fig. 1. Illustration of acoustically modulated optical pulses: (a) ideal pulse indicating no delay times between acoustic and optical signals, (b) amplitude modulated pulse induced by the free natural resonance vibrations of the fiber (τ_R is the resonance period) and (c) pulse with AOM phase-shifted peaks reducing effects of the natural resonance and decreasing the overall rise time of the optical signal. Dc is the duty cycle of the modulating acoustic pulse.

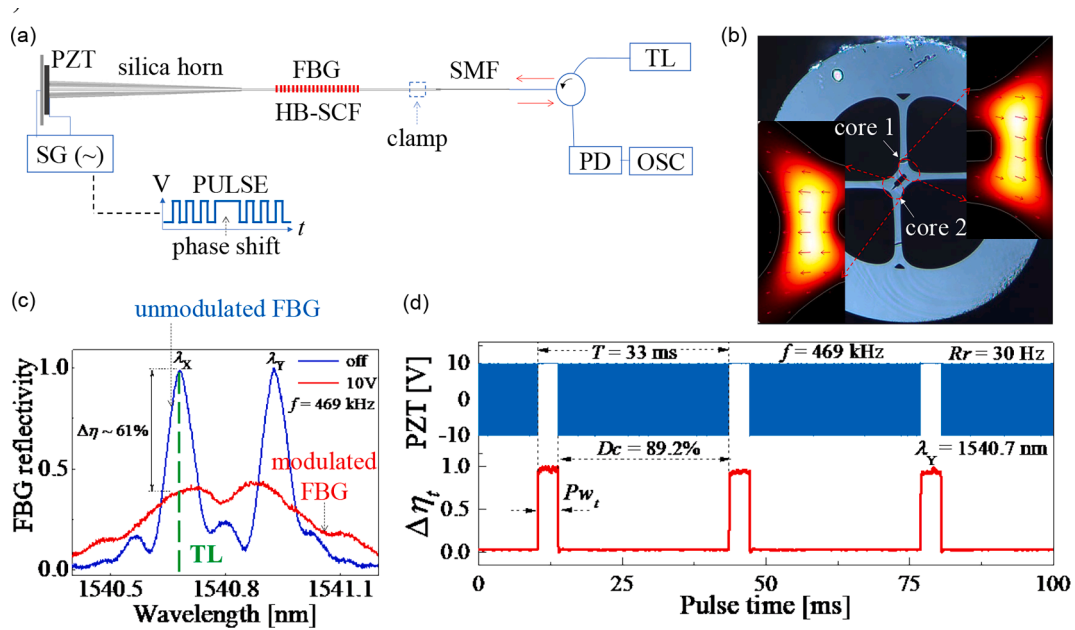


Fig. 2. Illustration of the (a) acousto-optic modulator with the experimental setup. (b) Highly birefringent suspended core fiber (HB-SCF) with a detail of the simulated power distribution of the fast X mode (the red arrows indicate the X polarization of the electric field in the fiber cores). (c) Measured unmodulated (blue) and modulated (red) spectrum of the fiber Bragg grating (FBG) inscribed in the HB-SCF. (d) Measured electrical pulse train applied to the PZT at $f = 469$ kHz (blue) and the acoustically modulated optical pulse at the duty cycle of $Dc = 89.2\%$ (red). (For interpretation of the references to colour in this figure legend, the reader is referred to the web version of this article.)

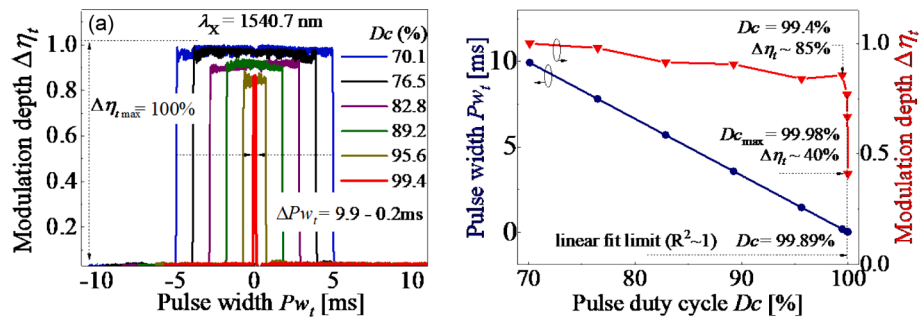


Fig. 3. (a) Temporal pulse width modulation of the FBG reflected optical power at the wavelength of $\lambda_x = 1540.7$ nm. The temporal widths are tuned by changing the duty cycle ON of the electrical pulse from $Dc = 70.1$ to 99.4% at a voltage of 10 V and frequency of $f = 469$ kHz applied to the PZT. (b) Variation of the pulse width P_{w_t} and modulation depth $\Delta\eta_t$ for the considered Dc range.

up to $Dc = 99.4\%$ (red graphic) in Fig. 3(b). The modulation depth slope in the range $Dc = 70.1$ – 99.4% is low due to the large time gaps between acoustic pulses (corresponding to the optical pulse width variations in Fig. 3(a) and (b) (dark blue graphic)).

The pulse rise time $\tau_{10-90\%}$ (10–90 % of the optical level) is also investigated, gradually decaying from 56 to 44 μs in the considered Dc range in Fig. 3(a) (further seen in Fig. 5(a)). From this point, both modulation depth $\Delta\eta$ and rise time $\tau_{10-90\%}$ abruptly decay with increasing Dc , as seen respectively in Figs. 3(b) and 5(a). A second experiment is performed to investigate the pulse properties from $Dc = 99.83$ to 99.98% (6 arbitrary steps). Fig. 4 shows the simulated (dashed blue curve) and measured (red curve) acoustically modulated optical pulses for the considered Dc range.

The simulated pulses are also averaged to emphasize the fundamental resonance peaks and compare with the measured pulses. Note in Fig. 4 that the amplitude modulation caused by the fiber's fundamental acoustic resonance induces peaks on the optical pulse envelope, which are more evident when Dc is switched OFF. The simulated peaks on the pulse's right side are used as reference to estimate the full resonance temporal period τ_R , as indicated in Fig. 1(b). Simulated and measured

values show good agreement mainly along the pulse fall time of $\tau_F = 13.3$ μs which is about one half-period of the resonance's complete sinusoidal cycle ($\tau_F = 0.5\tau_R$). The optical pulse fall time corresponds to the rise time of the acoustic strain when it is switched ON and emitted along the fiber. The measured and simulated resonance period of $\tau_R = 26.6$ μs agrees well with the analytically calculated $\tau_R = 26$ μs for the employed fiber length of 3.7 cm (considering $\tau_R = 4L(\rho/Y)^{1/2}$, $\rho = 2200$ kg/m^3 and $Y = 72.5$ GPa [25]).

The fundamental fiber vibration resonance has a sinusoidal wave profile, as indicated by the oscillations in Fig. 4(b) and illustrated in Fig. 1(b). Note that the wave maxima and minima induce peaks and notches in the pulse amplitude. During the switching OFF, the overlap of the out of phase transmitted and reflected acoustic pulses in the fiber, induces a phase shift in the resonance sinusoidal wave. Note in Fig. 4(a) that the wave period between the central resonance peaks is reduced, indicating a phase shift decreasing the resonance's pulse amplitude modulation and the rise time of the optical pulses (as illustrated in Fig. 1 (c)).

The decreasing temporal gaps between pulse trains reduce the peaks of the amplitude modulation. Note in Fig. 4(e) and (f) that no peaks are

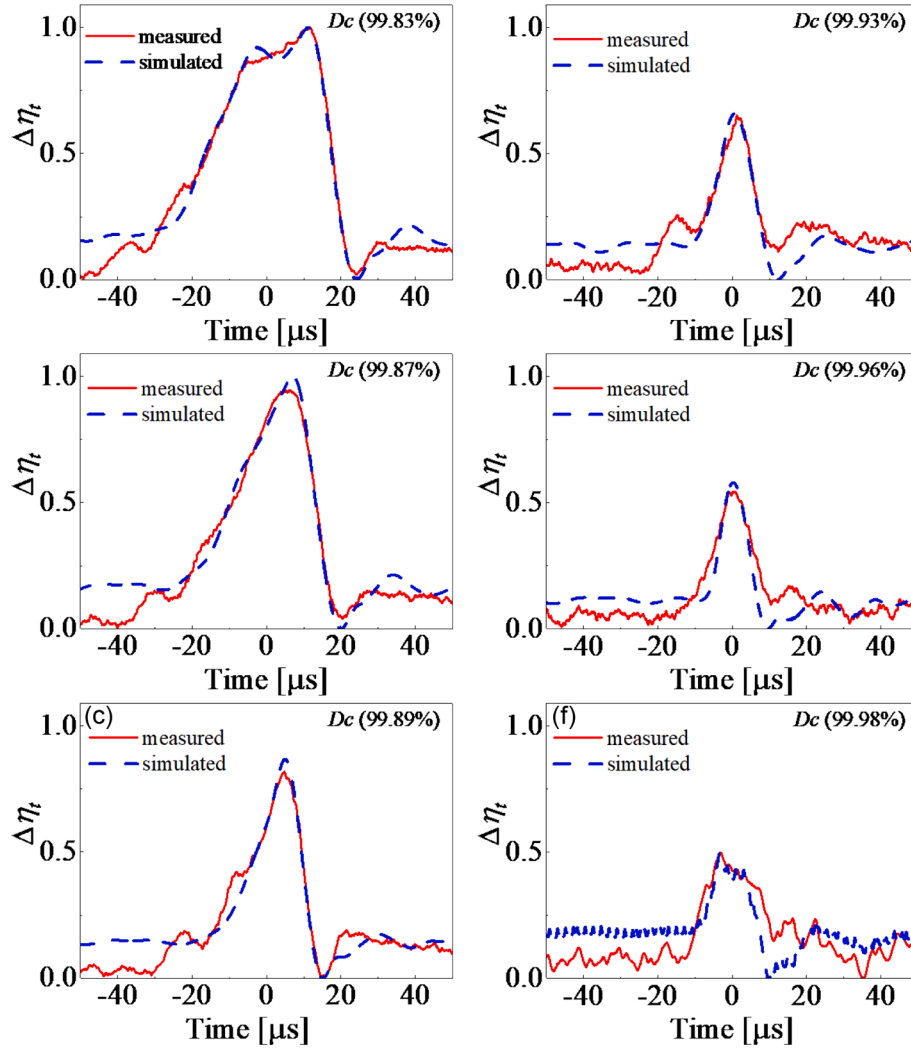


Fig. 4. Acousto-optic temporal control and shaping of optical pulses. The pulse rise time is gradually decreased by tuning the duty cycle ON of the applied electrical signal from (a)-(f) $D_c = 99.83$ to 99.98 %. The rectangular pulses in Fig. 3(a) are shaped into nearly triangular pulses. The fundamental resonance's amplitude modulation inducing peaks on the pulses' envelope is considerably damped with increasing D_c .

observed on the left side of the pulse. It is because the temporal gap between pulse trains is shorter than the resonance period τ_R . Consequently, the resonance modulation is minimized, further smoothing, and decreasing the rise time. However, additional shortening of this temporal gap does not allow the full amplitude recovery of even the main pulse peak, as shown in Fig. 4(f). The resulting pulse distortion induces an apparent pulse lengthening reversion at $D_c = 99.98$ %.

The pulses' rise time significantly decreases from $\tau_{1-100\%} = 56$ to 9 μs , as shown in Fig. 5(b). Fig. 5(c) shows the variation of the pulse width P_{W_t} with increasing D_c . As expected, the decreasing pulse width is limited by the rising and falling time of the device. In addition, increasing D_c does not allow the grating spectrum to completely recover between pulse trains, reducing the modulation depth $\Delta\eta_b$, as shown in Fig. 5(d).

We have also investigated the modulator's shortest response time. Fig. 6 shows the electrical pulse train applied to the PZT and the rise time $\tau_{1-100\%}$ of the optical pulse at $D_c = 99.98$ %. Both curves are normalized to their individual maximum amplitudes. Note that the PZT is polarized with a positive voltage to shift the phase of consecutive acoustic pulse trains in the fiber during D_c OFF. The rise time $\tau_{1-100\%} = 9$ μs still indicates remaining undamped oscillations in the grating. The delay between optical-electrical signals, $\tau_{DL} = 6.6$ μs , is related to the acoustic signal generation and propagation from the PZT to the grating, including the travel time along the horn and coupling adhesives.

Overall, our achieved switching time of $\tau_{ST} = 15.6$ μs is slightly shorter than that obtained with a 20 % smaller acousto-optic device [22]. It indicates that the demonstrated modulation technique is promising to reduce the time response of even larger devices, relieving requirements to fabricate complex small acoustic components. Although size reduction of the PZT, acoustic horn, grating and fiber length is still an option to shorten the overall switching time, the decreasing rise time shown here is mainly caused by the damping of the free natural oscillations remaining in the fiber.

4. Outlook and further applications

This study aims to contribute to the emerging technology of fiber-based acousto-optic devices (AOMs) which are a promising alternative to the current commercially available bulk acousto-optic devices based on crystals or doped glasses. In bulk based AOMs, the acoustic waves generated by a piezoelectric transducer change the material refractive index diffracting an input light beam passing through the acoustic field. Light from an input fiber should be collimated to couple into the crystal while the modulated light is usually focused on the output fiber. These coupling mechanisms generally require additional optical components, increasing the complexity, insertion losses and costs. Overall, bulk AOMs mostly work in transmission. In this context, the demonstrated

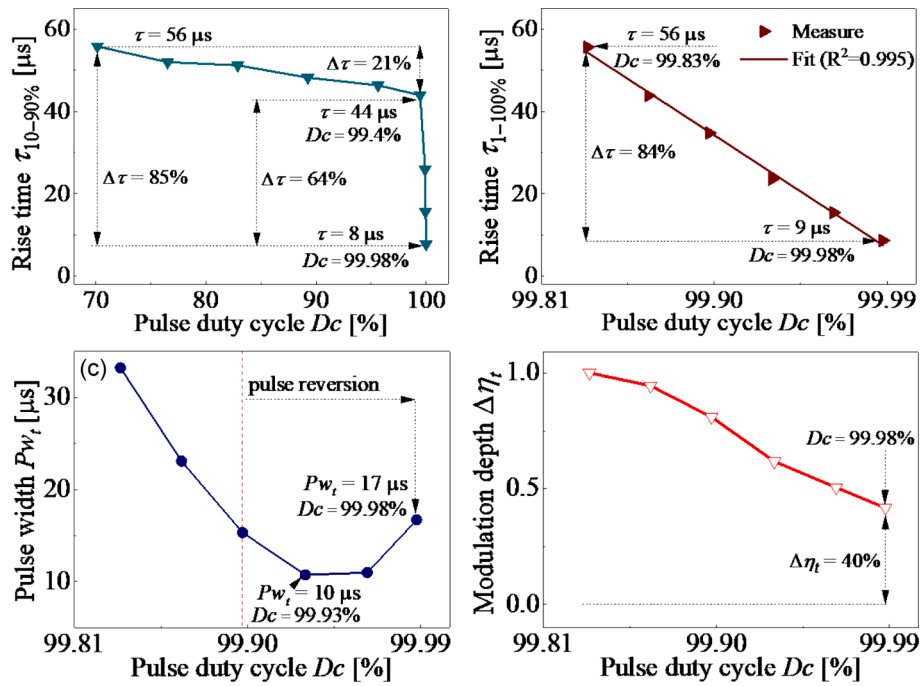


Fig. 5. (a) Pulse rise time $\tau_{10-90\%}$ for $D_c = 70.1-99.98\%$. (b) Rise time $\tau_{1-100\%}$, (c) pulse width Pw_t and (d) modulation depth $\Delta\eta_t$ for $D_c = 99.83-99.98\%$.

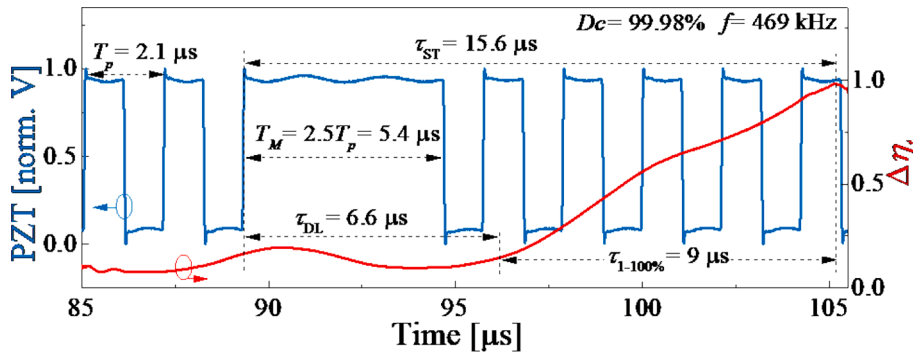


Fig. 6. Temporal response of the all-fiber acousto-optic device with details of the electrical pulse applied to the PZT (blue) and the modulated optical signal (red) at a duty cycle of $D_c = 99.98\%$ and frequency of $f = 469\text{ kHz}$. The temporal gap T_M is about 2.5 times the period of the applied electric pulse trains T_p . The sum of the pulse rise time $\tau_{1-100\%}$ and the delay between the optical and electrical signals τ_{DL} defines the overall device's switching time τ_{ST} . (For interpretation of the references to colour in this figure legend, the reader is referred to the web version of this article.)

all-fiber acousto-optic device provides the following features and benefits:

- Fiber optic monolithic configuration: the all-fiber AOM provides the best coupling and connection with existing fiber optic components and devices, reducing the optics, insertion losses, device size, which improves the overall device efficiency.
- Fiber Bragg grating: the employed FBG can be designed to provide up to 99 % reflection of the input light, enabling additional operation in reflection unlike the bulk modulators (additionally reducing losses and optics employed in the transmission output). Since the FBG is the effective component for acousto-optic modulation, the AOMs dimensions can be potentially considerably reduced to the grating length (few millimeters) and fiber core diameter (few micrometers).
- Highly birefringence suspended core fiber: this fiber used in our device provides significant reduction of the bulk silica in the fiber, which is an important benefit to improve the acousto-optic interaction with the FBG compared to other AOMs employing bulk solid fibers as SMFs. The HB-SCF has 2 birefringent cores which might

enable multiwavelength tunability of the optical pulses demonstrated in this study [28].

We evaluate just the temporal modulated properties of the HB-SCF and are essentially looking simultaneously at λ_x and λ_y , which are similarly coupled at the polarization state of 45° , so there was no need for any additional polarization control elements (this fiber provides high acousto-optic modulation efficiency because of the reduced silica content). Overall, considering that the HB-SCF structure is polarization sensitive and λ_x and λ_y are orthogonally polarized, the use of a polarization controller and acoustic excitation at higher frequencies might enable extra selective multiwavelength and polarization tuning of the optical pulses [28].

Compared to other fiber based AOMs, we conclude that the grating response is very fast because the acousto-optic device and modulation technique enables the grating to recover even when applying a very short temporal gap between consecutive acoustic pulses ($5.4\ \mu\text{s}$ time gap in blue signal – Fig. 6). This fast response reduces the effects of unwanted natural vibrations in the fiber, minimizing the peaks on the optical pulses and decreasing the device rise time when tuning D_c from

99.83 to 99.98 %. The compromise with reducing modulation depth can be balanced with proper tuning of D_c for a specific application. The speed of the acousto-optic devices is generally determined by the rise and switching times as shown in Fig. 6. Thus, our modulator providing a switching time of $\tau_{ST} = 15.6 \mu\text{s}$ is significantly faster compared to previous studies (40 to 500 μs [15,17–21]). The decreased rise/fall and switching times come from improvements and reduction of the whole acousto-optic device, composed of a small PZT (source), acoustic transmission path (reduced silica horn properly fabricated to match with the diameter of a highly efficient SCF), and target (short FBG). While the demonstrated modulation technique reduces the rise time, the improved modulator components and connections contribute also to reduce the delay time τ_{DL} of electrical and optical signals, shortening the overall switching time in Fig. 6.

The demonstrated AOM and modulation technique have potential application in the following fields:

- Fiber lasers for telecommunications, material processing, sensing and medicine, providing various advantages over other types of lasers, such as, compact and stable setup, and compatibility with the traditional optical fiber systems. The low losses and possibility of producing fiber cavities using FBGs provides lower pump thresholds and higher laser efficiencies. It is easy to move the fiber end without the need for directing optics requiring fine adjustment and alignment. The lasing is produced in a small diameter fiber core enabling high beam quality and focus on small spots, which is useful for micromarking, welding or metal microdrilling, or even heating microorganisms in biomedical applications. In these cases, our AOM might modulate and increase the repetition rate of pulsed Q-switched and mode-locked fiber lasers.
- Fiber sensors to measure and monitor fluid properties in industry (food, chemical, oil, automotive) and biomedicine, defining the texture, consistency, and quality of products, as well, pumping, mixing and transport of substances. Our AOM might be used to characterize viscosity, density, and refractive index by exposing the vibrating fiber to the desired substance [29,30]. The fluid induced damping of the acoustic wave amplitude changes the modulated grating spectrum and optical pulses, allowing characterizing the fluid properties. The time-dependent viscosity might be evaluated by changes of the pulse rise time caused by the fluid [29]. In this case, our modulator might significantly contribute to reduce the response time of current devices (few milliseconds) while reducing the overall device size (about 10 cm long).

5. Conclusion

We have demonstrated a new fast technique for acousto-optic generation and tuning of acoustically induced pulses in a SCF-FBG. An acoustic pulse train is switched ON/OFF out of phase along the fiber and the temporal response of the grating reflected optical pulses is experimentally and numerically characterized. The pulse's amplitude modulation caused by the natural fiber fundamental acoustic resonance is investigated in detail for the first time.

The good agreement between the experiment, simulations and theory strongly confirms the excitation of natural resonant vibrations in the fiber modulated by an acoustic signal with an abrupt step varying amplitude. The results show that the fundamental resonance induces peaks on the pulse envelope with a temporal period defined by the fiber length and material. This resonance effect is significantly reduced by shortening the temporal gap (duty cycle OFF) between consecutive acoustic pulse trains, which reflect at the modulator ends and interfere out of phase along the grating. For temporal gaps in the order or shorter than the resonance period, the pulse amplitude modulation and peaks are considerably reduced.

The demonstrated technique allows the tunable reduction of the response time of the acousto-optic device. The pulse width is modulated

from 9.9 ms to 10 μs , while keeping high pulse modulation depths. The pulse rise time is tuned from 56 to 9 μs , contributing to the shortest switching time of 15.6 μs . To the best of our knowledge, this is the fastest all-fiber acousto-optic device reported. The results indicate a promising technique to shape the pulsed temporal reflection of Bragg gratings, enabling fast modulation of fully reconfigurable all-fiber integrated devices.

Further advance of this study might suggest deep investigation of the destructive interference of the remaining resonance vibrations during duty cycle OFF. Optical pulses with narrower widths might be achieved with further damping or canceling of acoustic resonance effects. In this way, pulse shape profiles being adjusted by the amplitude and duty cycle of the applied acoustic signal are expected. It will also enable new opportunities to modulate the power of pulsed fiber lasers.

CRedit authorship contribution statement

Ricardo E. da Silva: Conceptualization, Methodology, Validation, Formal analysis, Investigation, Writing – original draft, Writing – review & editing. **Egor Manuylovich:** Writing – review & editing, Resources, Investigation, Formal analysis. **Namita Sahoo:** Writing – review & editing, Resources, Investigation, Formal analysis. **Marcos A.R. Franco:** Writing – review & editing, Supervision, Resources, Investigation, Funding acquisition, Formal analysis. **Hartmut Bartelt:** Writing – review & editing, Resources, Investigation, Formal analysis. **David J. Webb:** Writing – review & editing, Writing – original draft, Supervision, Resources, Investigation, Funding acquisition, Formal analysis.

Declaration of competing interest

The authors declare that they have no known competing financial interests or personal relationships that could have appeared to influence the work reported in this paper.

Data availability

Data will be made available on request.

Acknowledgements

This project has received funding from the European Union Horizon 2020 research and innovation programme under the Marie Skłodowska-Curie grant agreement No 713694, from 305321/2023-4, Conselho Nacional de Desenvolvimento Científico e Tecnológico (CNPq), and from grant #2022/10584-9, São Paulo Research Foundation (FAPESP).

References

- [1] W. Liu, M. Li, R.S. Guzzon, E.J. Norberg, J.S. Parker, M. Lu, L.A. Coldren, J. Yao, A fully reconfigurable photonic integrated signal processor, *Nat. Photonics* 10 (2016) 190–195.
- [2] R.-R. Xie, G.-Q. Qin, H. Zhang, M. Wang, G.-Q. Li, D. Ruan, G.-L. Long, Phase-controlled dual-wavelength resonance in a self-coupling whispering-gallery-mode microcavity, *Opt. Lett.* 46 (2021) 773.
- [3] L. Thévenaz, Slow and fast light in optical fibres, *Nat. Photonics* 2 (2008) 474–481.
- [4] J.T. Mok, C.M. de Sterke, B.J. Eggleton, Delay-tunable gap-soliton-based slow-light system, *Opt. Express* 14 (2006) 11987.
- [5] D. Janner, G. Galzerano, G. Della Valle, P. Laporta, S. Longhi, M. Belmonte, Slow light in periodic superstructure Bragg gratings, *Phys. Rev. E - Stat. Nonlinear, Soft Matter Phys.* 72 (2005) 056605.
- [6] A.D. Ellis, D.J. Richardson, M. Ibsen, P. Petropoulos, Rectangular pulse generation based on pulse reshaping using a superstructured fiber Bragg grating, *J. Light. Technol.* 19 (5) (2001) 746–749.
- [7] M. Li, D. Janner, J. Yao, V. Pruneri, Arbitrary-order all-fiber temporal differentiator based on a fiber Bragg grating: design and experimental demonstration, *Opt. Express* 17 (2009) 19798.
- [8] M. Li, J. Yao, All-fiber temporal photonic fractional Hilbert transformer based on a directly designed fiber Bragg grating, *Opt. Lett.* 35 (2010) 223.
- [9] A. Arora, M. Esmaelpour, M. Bernier, M.J.F. Dignonnet, High-resolution slow-light fiber Bragg grating temperature sensor with phase-sensitive detection, *Opt. Lett.* 43 (2018) 3337.

- [10] M. Delgado-Pinar, A. Díez, J.L. Cruz, M.V. Andrés, Single-frequency active Q-switched distributed fiber laser using acoustic waves, *Appl. Phys. Lett.* 90 (2007) 171110.
- [11] G. Lenz, B.J. Eggleton, C.K. Madsen, R.E. Slusher, Optical delay lines based on optical filters, *IEEE J. Quantum Electron.* 37 (2001) 525–532.
- [12] J. Azaña, L.R. Chen, Synthesis of temporal optical waveforms by fiber Bragg gratings: a new approach based on space-to-frequency-to-time mapping, *J. Opt. Soc. Am. B* 19 (2002) 2758.
- [13] P. Xue, Q. Liu, Z. Wu, Q. Wua, C. Zhao, W.P. Ng, R. Fu, R. Binns, Electrically tuning characteristics of 1c selectively infiltrated PCF Sagnac interferometer, *IEEE Photonics Technol. Lett.* (2021).
- [14] R.E. Silva, T. Tiess, M. Becker, T. Eschrich, M. Rothhardt, M. Jäger, A.A.P. Pohl, All-fiber 10 MHz acousto-optic modulator of a fiber Bragg grating at 1060 nm wavelength, *Opt. Express.* (2015).
- [15] M. Delgado-Pinar, J. Mora, A. Díez, J.L. Cruz, M.V. Andrés, Wavelength-switchable fiber laser using acoustic waves, *IEEE Photonics Technol. Lett.* 17 (2005) 552–554.
- [16] R.E. Silva, M.A.R. Franco, P.T. Neves, H. Bartelt, A.A.P. Pohl, P. Neves Jr., H. Bartelt, A.A.P. Pohl, Detailed analysis of the longitudinal acousto-optical resonances in a fiber Bragg modulator, *Opt. Express* 21 (2013) 6997–7007.
- [17] Y. Li, L. Huang, H. Han, L. Gao, Y. Cao, Y. Gong, W. Zhang, F. Gao, L.P. Ikehukwu, T. Zhu, Acousto-optic tunable ultrafast laser with vector-mode-coupling-induced polarization conversion, *Photonics Res.* 7 (2019) 798.
- [18] H.S. Park, K.Y. Song, S.H. Yun, B.Y. Kim, All-fiber wavelength-tunable acousto-optic switches based on intermodal coupling in fibers, *J. Light. Technol.* 20 (2002) 1864–1868.
- [19] C.A.F. Marques, R.A. Oliveira, A.A.P. Pohl, J. Canning, R.N. Nogueira, Dynamic control of a phase-shifted FBG through acousto-optic modulation, *Opt. Commun.* 284 (2011) 1228–1231.
- [20] M. Delgado-Pinar, D. Zalvidea, A. Díez, P. Perez-Millan, M. Andres, Q-switching of an all-fiber laser by acousto-optic modulation of a fiber Bragg grating, *Opt. Express* 14 (2006) 1106–1112.
- [21] A. Díez, M. Delgado-Pinar, J. Mora, J.L. Cruz, M.V. Andrés, Dynamic fiber-optic add-drop multiplexer using Bragg gratings and acousto-optic-induced coupling, *IEEE Photonics Technol. Lett.* 15 (2003) 84–86.
- [22] R.E. Silva, E. Manuylovich, N. Sahoo, M. Becker, M. Rothhardt, H. Bartelt, D. J. Webb, Highly efficient side-coupled acousto-optic modulation of a suspended core fiber Bragg grating, *IEEE Photonics Technol. Lett.* 33 (2021) 1379–1382.
- [23] A.A.P. Pohl, R.A. Oliveira, R.E. Silva, C.A.F. Marques, P.T. de Neves, K. Cook, J. Canning, R.N. Nogueira, Advances and new applications using the acousto-optic effect in optical fibers, *Photonic Sens.* 3 (2013) 1–25.
- [24] R.E. Silva, T. Tiess, M. Becker, T. Eschrich, M. Rothhardt, M. Jäger, A.A.P. Pohl, H. Bartelt, Acousto-optic modulation of a fiber Bragg grating in suspended core fiber for mode-locked all-fiber lasers, *Laser Phys. Lett.* 12 (2015) 045101.
- [25] P.T. Neves Jr., A.A.P. Pohl, Time analysis of the wavelength shift in fiber Bragg gratings, *J. Light. Technol.* 25 (2007) 3580–3588.
- [26] M. Becker, J. Bergmann, S. Brückner, M. Franke, E. Lindner, M.W. Rothhardt, H. Bartelt, Fiber Bragg grating inscription combining DUV sub-picosecond laser pulses and two-beam interferometry, *Opt. Express* 16 (2008) 19169.
- [27] M. Bello-Jiménez, C. Cuadrado-Laborde, A. Díez, J.L. Cruz, M.V. Andrés, Experimental study of an actively mode-locked fiber ring laser based on in-fiber amplitude modulation, *Appl. Phys. B* 105 (2011) 269–276.
- [28] R.E. Silva, M. Becker, M. Rothhardt, H. Bartelt, A.A.P. Pohl, Electrically tunable multiwavelength bragg grating filter acoustically induced in a highly birefringent suspended core fiber, *IEEE Photonics J.* 9 (1) (2017) 1–9.
- [29] R.A. Oliveira, J. Canning, K. Cook, M. Nashqbandi, A.A.P. Pohl, Compact dip-style viscometer based on the acousto-optic effect in a long period fiber grating, *Sens. Actuators B: Chem.* 157 (2) (2011) 621–626.
- [30] H. Qian, et al., Fiber-optic viscometer with all-fiber acousto-optic superlattice modulated structure, *J. Lightwave Technol.* 36 (18) (2018) 4123–4128.